The following article appeared in AIP Advances 8, 101410 (2018); and may be found at: https://doi.org/10.1063/1.5041954

AIP Advances

Magnetic and martensitic transformations in $Ni_{48}Co_2Mn_{35}In_{15}$ melt-spun ribbons

Cite as: AIP Advances **8**, 101410 (2018); https://doi.org/10.1063/1.5041954
Submitted: 28 May 2018 . Accepted: 14 August 2018 . Published Online: 30 August 2018

Sudip Pandey, Abdiel Quetz, P. J. Ibarra-Gaytan, C. F. Sanchez-Valdes, Anil Aryal, Igor Dubenko, J. L. Sanchez Llamazares, Shane Stadler, and Naushad Ali

Magnetic and martensitic transformations in $Ni_{48}Co_2Mn_{35}In_{15}$ melt-spun ribbons

Sudip Pandey,[1,a] Abdiel Quetz,[1] P. J. Ibarra-Gaytan,[2,3]
C. F. Sanchez-Valdes,[4] Anil Aryal,[1] Igor Dubenko,[1]
J. L. Sanchez Llamazares,[2,a] Shane Stadler,[5] and Naushad Ali[1]
[1]*Department of Physics, Southern Illinois University, Carbondale, Illinois 62901, USA*
[2]*Instituto Potosino de Investigación Cientıfica y Tecnológica A.C., Camino a la Presa San Jose 2055, Col. Lomas 4a Sección, San Luis Potosı, S.L.P. 78216, Mexico*
[3]*Institute of Physics, Faculty of Sciences, University Pavol Jozef Safárik, Park Angelinum 9, 04154 Kosice, Slovakia*
[4]*División Multidisciplinaria, Ciudad Universitaria, Universidad Autónoma de Ciudad Juárez (UACJ), Calle José de Jesús Macías Delgado # 18100, Ciudad Juárez, Chihuahua 32579, Mexico*
[5]*Department of Physics & Astronomy, Louisiana State University, Baton Rouge, Louisiana 70803, USA*

(Received 28 May 2018; accepted 14 August 2018; published online 30 August 2018)

As-solidified $Ni_{48}Co_2Mn_{35}In_{15}$ ribbons were prepared through the melt-spinning method, and their structural, magnetic, magnetocaloric properties, and martensitic transformations were investigated. The inverse martensitic transformation temperature (T_A=325 K) for the melt spun ribbons shifted by 55 K to higher temperature relative to that of the bulk material (T_A = 270 K). The working temperature range of the magnetic entropy change (ΔS_M) in $Ni_{48}Co_2Mn_{35}In_{15}$ ribbons has been significantly expanded relative to that of bulk. The roles of the magnetostructural transitions on the magneto-responsive properties of the ribbons are discussed.
https://doi.org/10.1063/1.5041954

INTRODUCTION

In the last ten years, the structural, magnetic, and magnetocaloric properties of off-stoichiometric Ni-Mn-X based Heusler alloys (X= Sn, In, Sb) in the form of ribbons have been extensively investigated.[1–10] They have been fabricated by rapid quenching using the melt-spinning technique, which is an effective one-step and low-cost mechanism to produce the ribbons with a cooling rate of 10^5 K/s (with thickness of about 10-50 μm). The method also eliminates the high-temperature, long term thermal annealing needed to obtain a single phase in these alloys. Rapid solidification has a stronger influence on the resulting microstructure, and therefore on the temperature of the phase transitions and related magnetoresponsive properties of the alloys. In fact, by changing the synthesis parameters, the phase transition temperatures and magnetic properties of melt-spun ribbons may change considerably as compared to their bulk counterparts.[11–14] In practice, the melt spinning technique is another tool used to tune the magnetic properties and magnetocaloric effects (MCE) of Heusler alloys.

It was reported that the substitution of a small amount of Co in bulk $Ni_{48}Co_2Mn_{35}In_{15}$ Heusler alloys shifts the phase transition temperatures (T_A) by about 40 K and Curie temperature of austenite (T_C) by about 30 K toward lower and higher temperatures, respectively.[15] Large magnetocaloric parameters (ΔS_M= 21 J kg^{-1} K^{-1}, and adiabatic temperature change, ΔT_{ad}= -3.7 K, for a magnetic field change $\mu_o \Delta H$ =5 T), and a giant magnetoresistance (70%) were observed in these

[a]Corresponding author: e-mail: sudip@siu.edu (Sudip Pandey) and jose.sanchez@ipicyt.edu.mx (J. L. Sánchez Llamazares)

systems through the structural transition.[15,16] Hence, in order to develop better magnetocaloric materials with reduced dimensions, we have conducted a detailed characterization of the magnetocaloric properties (ΔS_M, refrigerant capacity (RC), and magnetic field-induced hysteresis loss (HL)) through the inverse martensitic transformation (MT) for as-solidified $Ni_{48}Co_2Mn_{35}In_{15}$ melt-spun ribbons.

EXPERIMENTAL TECHNIQUES

A 3 g ingot of nominal composition $Ni_{48}Co_2Mn_{35}In_{15}$ was prepared by arc-melting in a high-purity argon atmosphere from 4N purity elements Ni, Co, Mn, and In. The ingot was re-melted several times and annealed at 1123 K for 48 hours under high vacuum and then slowly cooled to room temperature. This arc melted sample was used to produce rapidly solidified melt-spun ribbons with thicknesses of 30–35 μm using a Edmund Buhler model SC melt spinner system at a linear speed v = 20 m/s of the rotating Cu wheel. The structural characterization of the ribbons sample was done at room temperature by using a high resolution Rigaku Smartlab diffractometer powder employing Cu-K_α radiation. The patterns were measured on a finely powdered sample. The magnetic properties of the ribbons were measured using a 9 T Quantum Design PPMS® Dynacool® platform with the VSM option in a temperature range of 5 K to 400 K. The ribbon samples studied were directly glued to the quartz VSM sample holder using GE-7031 varnish. An external magnetic field $\mu_o H$ was applied along the major ribbon length, or rolling direction of the ribbon, in order to minimize the internal demagnetizing field. Additional details of the sample preparation and measurements of ribbons can be found elsewhere.[17]

RESULTS AND DISCUSSION

Fig. 1 shows the room temperature X-ray powder diffraction pattern obtained for the as-solidified melt-spun ribbons. The XRD pattern shows the coexistence of austenitic and martensitic phases. Their crystal structures are consistent with those previously reported for bulk $Ni_{48}Co_2Mn_{35}In_{15}$ alloys,[15] and can be described as a mixture of tetragonal (martensitic) and cubic (austenitic) crystal structural phases.

The temperature dependence of zero-field-cooled (ZFC) and field cooled (FC) magnetization M(T) curves under static magnetic fields of 5 mT and 5 T for a $Ni_{48}Co_2Mn_{35}In_{15}$ ribbons are shown in Fig. 2. The heating/cooling temperature sweep rate employed was 1.5 $Kmin^{-1}$. The Curie temperature is found to be around 312 K at 5 mT (see the M(T) curve on cooling in Figure 2(a)). The application of a large magnetic field of 5 T results in a shift of the martensitic and magnetic transitions to lower temperature (by about 6 K) and high temperature (by about 38 K), respectively. The Curie temperature of the austenitic phase (T_C) observed at μ_0H=5 T remains similar to that of the bulk. With $\mu_0 H$ = 5 T, a moderate jump in the magnetization (ΔM = 40 A m^2 kg^{-1}) was observed across the

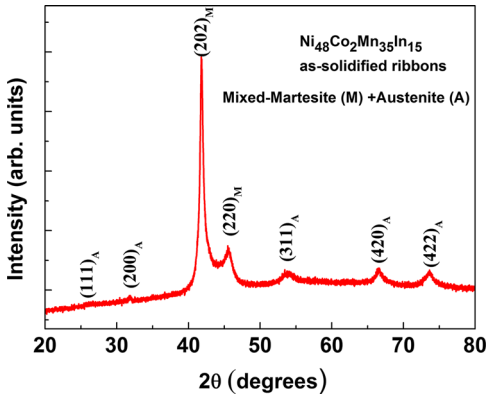

FIG. 1. Room temperature X-ray powder diffraction pattern obtained for an as-solidified $Ni_{48}Co_2Mn_{35}In_{15}$ melt-spun ribbons.

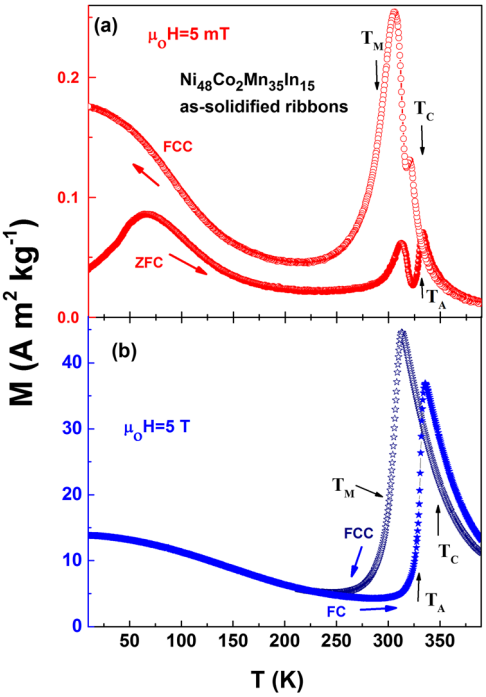

FIG. 2. Temperature dependence of the ZFC and FC magnetization curves under static magnetic fields of (a) 5 mT and (b) 5 T for an as-solidified $Ni_{48}Co_2Mn_{35}In_{15}$ melt-spun ribbons.

inverse martensitic transformation, as shown in Figure 2(b). It can be observed from Figure 2(a) that the martensitic transition takes place at $T=T_M<T_C$ on cooling and the magnetic ordering temperature of the austenite is less than the temperature of the structural transition, T_A. Thus, the transition from the martensitic to the paramagnetic austenite phase can be detected at 5 mT with increasing temperature. A temperature hysteresis in the magnetization has been observed in the vicinity of the structural and magnetic transformations at low and high magnetic fields (see Figure 2). Such behavior is rather rare, and results when $T_M<T_C<T_A$ (as in Figure 2(a)). The splitting of the low field ZFC and FC M(T) curves at lower temperatures indicates magnetic frustration as has observed in most of Ni-Mn-X based Heusler alloys with X=Sn, In, and Sb.[12–14]

To examine the nature of the phase transitions, Arrott plots, i.e., M^2 versus μ_oH/M plots, across the inverse martensitic and Curie transition temperatures were constructed and shown in Figure 3(a). The S-shaped curves with negative slope in the Arrott plots through the inverse martensitic transition is a signature of the first-order nature of the phase transition. On the contrary, positive slope curves confirm the second-order transition and the Curie temperature.

Isothermal magnetization curves for an as-solidified $Ni_{48}Co_2Mn_{35}In_{15}$ melt-spun ribbons measured up to a maximum magnetic field of μ_oH_{max}=5 T are shown in Figure 3(b). The magnetization isotherms exhibit characteristic features of a weak metamagnetic transition from a lower magnetization martensitic phase to a higher magnetization austenitic phase near the inverse martensitic transition. At higher temperatures, the magnetization curves show a paramagnetic-like behavior. It should be noted that the isothermal magnetization curves for $Ni_{48}Co_2Mn_{35}In_{15}$ ribbon as shown in Figure 3(b) are similar to those observed for the bulk material.[15]

Magnetic-field-induced hysteresis, an unwanted characteristic in a magnetic refrigerant material, occurs at the first order transition. To estimate the hysteresis loss in the $Ni_{48}Co_2Mn_{35}In_{15}$ melt-spun ribbons at inverse martensitic transition, a set of successive isothermal magnetization curves were measured in 1 K increments for both magnetizing (from 0 to 5 T) and demagnetizing (from 5 to 0 T) fields as shown in Figure 4(a). The hysteresis loss (HL) was estimated from the enclosed area between the magnetizing and demagnetizing $M(\mu_oH)$ curves and plotted in the inset of Figure 4(a). The average hysteresis loss <HL> at 5 T between 321 and 329 K is -13.7 J kg^{-1}. The obtained

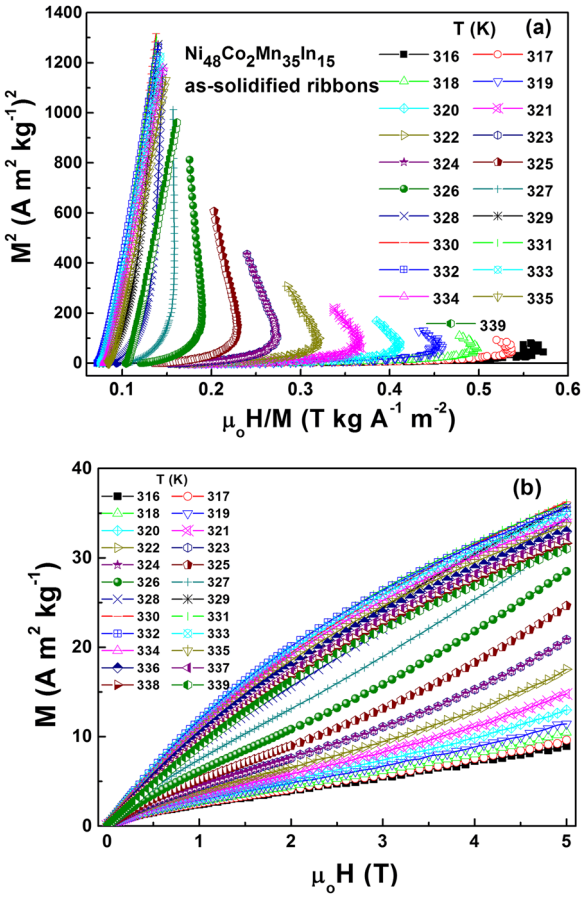

FIG. 3. (a) Arrott plots for selected temperatures across the inverse martensitic and Curie transitions and (b) isothermal magnetization curves measured up to a maximum magnetic field of 5 T for an as-solidified $Ni_{48}Co_2Mn_{35}In_{15}$ melt-spun ribbons.

value of the HL for as-spun ribbons is significantly less than that of bulk $Ni_{48}Co_2Mn_{35}In_{15}$ [<HL> = 81 J kg^{-1}].[16]

Figure 4(b) shows the thermal dependence of the field-induced magnetic entropy change (ΔS_M) of a $Ni_{48}Co_2Mn_{35}In_{15}$ melt-spun ribbons estimated from the magnetization isotherms using the Maxwell relation. An inverse MCE (positive $\Delta S_M{}^{peak}$) and direct MCE (negative $\Delta S_M{}^{peak}$) with values of 12.1 J kg^{-1} K^{-1} and 3.0 J kg^{-1} K^{-1} for a magnetic field of 5 T, were obtained at the inverse martensitic transition and the Curie temperatures, respectively. The MCE parameters were found to be smaller than those of bulk $Ni_{48}Co_2Mn_{35}In_{15}$ ($\Delta S_M{}^{peak}$= 21 J kg^{-1} K^{-1}) and other Ni-Mn-In based Heusler alloys.[16–18] However, the working temperature, in terms of the full-width at half maximum of the $\Delta S_M(T)$ curve, δT_{FWHM}, for the synthesized ribbons has been significantly expanded. The significantly lower magnetic hysteresis and larger working temperature range makes $Ni_{48}Co_2Mn_{35}In_{15}$ melt-spun ribbons a better magnetocaloric materials than its bulk counterpart. Melt-spinning effectively promotes more homogeneous materials with improved MCE properties.

The refrigerant capacity (RC) has been estimated employing three different protocols. The product $|\Delta S_M{}^{peak}| \times \delta T_{FWHM}$ (referred as RC-1), where $\delta T_{FWHM} = T_{hot} - T_{cold}$, corresponds to the full-width at half-maximum of the $\Delta S_M(T)$ curve; (b) the area under the $\Delta S_M(T)$ curve between T_{hot} and T_{cold} (RC-2); and (c) maximum the product $\Delta S_M \times \delta T$ below the $\Delta S_M(T)$ curve (RC-3), which is known as the Wood and Potter criterion,[19] and plotted as a function of the magnetic field up to 5 T in the inset of Figure 4(b). RC values of 78.3 J/kg (*RC*-1), 63.2 J/kg (*RC*-2), and 39.5 J/kg (*RC*-3) were obtained for a field change of 5 T. This value of RC is smaller than those of the bulk Ni-Mn-In-B system.[20] The RC values and related magnetocaloric parameters are listed in Table I.

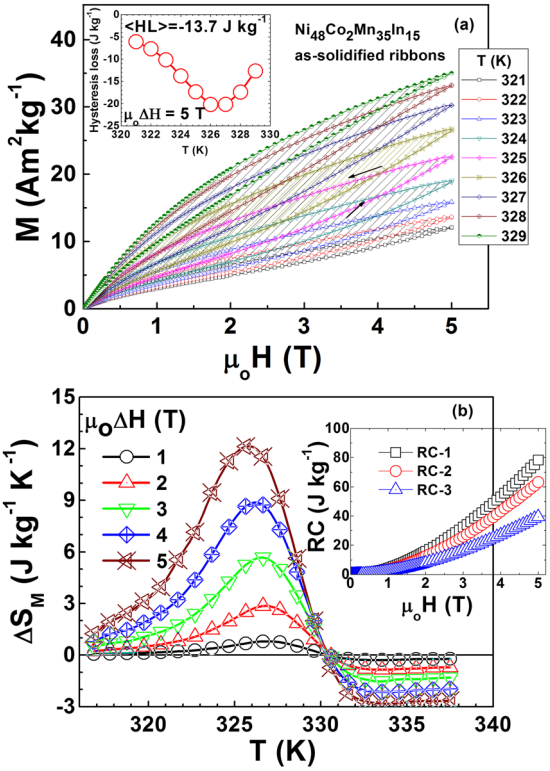

FIG. 4. (a) Magnetization isotherms measured during increasing and decreasing magnetic fields, and (b) magnetic entropy change as a function of temperature and field for an as-solidified $Ni_{48}Co_2Mn_{35}In_{15}$ melt-spun ribbons. The inset of (a) shows the hysteresis loss across the phase transition for a magnetic field change $\mu_o H_{max}$ = 5 T (heating protocol). The inset of (b) shows the refrigeration capacity (RC-1, RC-2, and RC-3) as a function of magnetic field change.

TABLE I. Peak magnetic entropy change ΔS_M^{peak}, *RC*-1, *RC*-2, δT_{FWHM}, T_{hot}, T_{cold}, *RC*-3, $\delta T^{RC\text{-}3}$, and $T_{hot}^{RC\text{-}3}$ and $T_{cold}^{RC\text{-}3}$ (related to *RC*-3) across the inverse martensitic transformation for as-solidified $Ni_{48}Co_2Mn_{35}In_{15}$ melt-spun ribbons.

$\mu_o\Delta H$ (T)	1	2	3	4	5
$\lvert\Delta S_M^{peak}\rvert$ (J kg^{-1} K^{-1})	0.8	2.9	5.7	8.7	12.1
RC-1 (J kg^{-1})	4.2	15	32	53	78
RC-2 (J kg^{-1})	3	13	26	43	63
<*HL*> (J kg^{-1})	-	-	-	-	14
δT_{FWHM} (K)	5	6	6	6	6
T_{hot} (K)	329	329	329	328	329
T_{cold} (K)	324	324	323	322	322
RC-3 (J kg^{-1})	2.0	8.0	16	27	4
$\delta T^{RC\text{-}3}$ (K)	5.1	5	5	5	5
$T_{hot}^{RC\text{-}3}$ (K)[a]	329	329	328	328	328
$T_{cold}^{RC\text{-}3}$ (K)[a]	324	324	324	323	323

[a]Related to RC-3.

CONCLUSIONS

In summary, we have investigated the magnetic and magnetoresponsive properties of $Ni_{48}Co_2Mn_{35}In_{15}$ melt-spun ribbons and compared the results to those of the corresponding bulk alloy. The significantly lower hysteresis, the position of transition near room temperature, and the large temperature range of the significant magnetic entropy change are the main distinctive magnetocaloric features of $Ni_{48}Co_2Mn_{35}In_{15}$ melt-spun ribbons.

ACKNOWLEDGMENTS

This work was supported by the Office of Basic Energy Sciences, Material Science Division of the U.S. Department of Energy, DOE Grant No. DE-FG02-06ER46291 (SIU) and DE-FG02-13ER46946 (LSU). The authors acknowledge the financial support received from Laboratorio Nacional de Investigaciones en Nanociencias y Nanotecnología (LINAN, IPICyT) in particular from M.Sc. B.A. Rivera-Escoto. C.F. Sánchez-Valdés is grateful to DMCU-UACJ for supporting his research activity under program PFCE and academic mobility grant, and also for the financial support received from PRODEP-SEP, Mexico (Grant No. UACJ- PTC-383).

[1] Z. B. Li, J. L. Sánchez Llamazares, C. F. Sánchez-Valdés, Y. D. Zhang, C. Esling, X. Zhao, and L. Zuo, Appl. Phys. Lett. **100**, 174102 (2012).
[2] Z. Li, Y. Zhang, C. F. Sánchez-Valdés, J. L. Sánchez Llamazares, C. Esling, X. Zhao, and L. Zuo, Appl. Phys. Lett. **104**, 044101 (2014).
[3] R. Caballero-Flores, T. Sánchez, W. O. Rosa, J. García, L. González-Legarreta, D. Serantes, V. M. Prida, Ll. Escoda, J. J. Suñol, and B. Hernando, J. Alloys Compd. **545**, 216 (2012).
[4] V. V. Sokolovskiy, V. D. Buchelnikov, S. V. Taskaev, V. V. Khovaylo, M. Ogura, and P. Entel, J. Phys. D, Appl. Phys. **46**, 305003 (2013).
[5] B. Hernando, J. L. Sánchez Llamazares, J. D. Santos, V. M. Prida, D. Baldomir, D. Serantes, R. Varga, and J. González, Appl. Phys. Lett. **92**, 132507 (2008).
[6] A. M. Aliev, A. B. Batdalov, I. K. Kamilov, V. V. Koledov, V. G. Shavrov, V. D. Buchelnikov, J. García, V. M. Prida, and B. Hernando, Appl. Phys. Lett. **97**, 212505 (2010).
[7] M. K. Ray, K. Bagani, R. K. Singh, B. Majumdar, and S. Banerjee, J. Appl. Phys. **114**, 123904 (2013).
[8] W. Guan, Q. R. Liu, B. Gao, S. Yang, Y. Wang, M. W. Xu, Z. B. Sun, and X. P. Song, J. Appl. Phys. **109**, 07A903 (2011).
[9] S. Pandey, A. Quetz, P. J. Ibarra-Gaytan, C. Sánchez-Valdes, A. Aryal, I. Dubenko, J. L. Sánchez Llamazares, S. Stadler, and N. Ali, AIP Adv. **8**, 056434 (2018).
[10] S. C. Ma, H. C. Xuan, C. L. Zhang, L. Y. Wang, Q. Q. Cao, D. H. Wang, and Y. W. Du, Appl. Phys. Lett. **97**, 052506 (2010).
[11] V. A. Chernenko, E. Cesari, J. Pons, and C. Segui, J. Mater. Res. **15**, 1496 (2000).
[12] O. Heczko, P. Švec, D. Jani, and K. Ullakko, IEEE Trans. Magn. **38**, 2841 (2002).
[13] A. Quintana-Nedelcos, J. L. Sánchez-Llamazares, D. Ríos-Jara, A. G. Lara-Rodríguez, and T. García-Fernández, Phys. Status Solidi **210**, 2159 (2013).
[14] V. V. Khovaylo, V. V. Koledov, D. I. Kuchin, V. G. Shavrov, N. N. Resnina, H. Miki, J. J. Suñol, and B. Hernando, IEEE Trans. Magn. **50**, 2501203 (2014).
[15] A. K. Pathak, I. Dubenko, Y. Xiong, P. W. Adams, S. Stadler, and N. Ali, J. Appl. Phys. **109**, 07A916 (2011).
[16] A. K. Pathak, I. Dubenko, C. Pueblo, P. Basnyat, S. Stadler, and N. Ali, IEEE Trans. Magn. **46**, 6 (2010).
[17] S. Pandey, A. Quetz, I. D. Rodionov, A. Aryal, M. I. Blinov, I. S. Titov, V. N. Prudnikov, A. B. Granovsky, I. Dubenko, S. Stadler, and N. Ali, J. Appl. Phys. **117**, 183905 (2015).
[18] S. Pandey, A. Quetz, A. Aryal, I. Dubenko, D. Mazumdar, S. Stadler, and N. Ali, Magnetochemistry **3**, 3 (2017).
[19] M. E. Wood and W. H. Potter, Cryogenics **25**, 667 (1985).
[20] S. Pandey, A. Quetz, P. J. Ibarra-Gaytan, C. Sánchez-Valdes, A. Aryal, I. Dubenko, J. L. Sánchez Llamazares, D. Mazumdar, S. Stadler, and N. Ali, J. Alloys Compd. **731**, 678–684 (2018).